

UC Irvine

UC Irvine Previously Published Works

Title

Knowledge-based three-dimensional dose prediction for tandem-and-ovoid brachytherapy.

Permalink

<https://escholarship.org/uc/item/6q10k742>

Journal

Brachytherapy, 21(4)

ISSN

1538-4721

Authors

Cortes, Katherina G
Kallis, Karoline
Simon, Aaron
[et al.](#)

Publication Date

2022-07-01

DOI

10.1016/j.brachy.2022.03.002

Copyright Information

This work is made available under the terms of a Creative Commons Attribution License, available at <https://creativecommons.org/licenses/by/4.0/>

Peer reviewed

1 **A knowledge-based organ dose prediction tool for**
2 **brachytherapy treatment planning of cervical cancer**
3 **patients**

4

5

6

7

8

9

10

11

12

13

14

15

16

17

18

19

20

21

22

23

Abbreviations: BT = brachytherapy, DVH = dose-volume histogram, EBRT = external beam radiotherapy, GYN = gynecologic, HRCTV = high-risk clinical target volume, IMRT = intensity-modulated radiation therapy, OAR = organ-at-risk, T&O = tandem-and-ovoid

25 **Purpose:** To explore knowledge-based organ-at-risk (OAR) dose estimation for
26 intracavitary brachytherapy planning for cervical cancer. Using established external-beam
27 knowledge-based dose-volume histogram (DVH) estimation methods, we sought to predict
28 bladder, rectum, and sigmoid D_{2cc} for tandem-and-ovoid treatments.

29 **Methods:** 136 loco-regionally advanced cervical cancer patients treated with 456
30 (356:100 training:validation ratio) CT-based tandem-and-ovoid brachytherapy fractions were
31 analyzed. Single fraction prescription doses were 5.5-8 Gy with dose criteria for the high-risk
32 clinical target volume (HRCTV), bladder, rectum and sigmoid. DVH estimations were obtained
33 by subdividing training set OARs into HRCTV boundary distance sub-volumes and computing
34 cohort-averaged differential DVHs. Full DVH estimation was then performed on the training and
35 validation sets. Model performance was quantified by $\Delta D_{2cc} = D_{2cc}(\text{actual}) - D_{2cc}(\text{predicted})$ (mean
36 and standard deviation). ΔD_{2cc} between training and validation sets were compared with a
37 Student's t-test ($p < 0.01$ significant). Categorical variables (physician, fraction-number, total
38 fractions, case complexity) that might explain model variance were examined using an ANOVA
39 test (Bonferroni-corrected $p < 0.01$ threshold).

40 **Results:** Training set deviations were bladder $\Delta D_{2cc} = -0.04 \pm 0.61$ Gy, rectum $\Delta D_{2cc} =$
41 0.02 ± 0.57 Gy and sigmoid $\Delta D_{2cc} = -0.05 \pm 0.52$ Gy. Model predictions on validation set did not
42 statistically differ: bladder $\Delta D_{2cc} = -0.02 \pm 0.46$ Gy ($p = 0.80$), rectum $\Delta D_{2cc} = -0.007 \pm 0.47$ Gy
43 ($p = 0.53$), and sigmoid $\Delta D_{2cc} = -0.07 \pm 0.47$ Gy ($p = 0.70$). The only significant categorical variable
44 was attending physician for bladder and rectum ΔD_{2cc} .

45 **Conclusion:** A simple boundary distance-driven knowledge-based DVH estimation
46 exhibited promising results in predicting critical brachytherapy dose metrics. Future work will

47 examine the utility of these predictions for quality control and automated brachytherapy
48 planning.

49 **Key Words:** knowledge-based planning, cervical cancer, dose predictions, machine learning,
50 quality control, treatment planning

51

52 **Introduction**

53 Brachytherapy (BT) is an essential component of cervical cancer treatment, which has
54 been linked to improved pelvic control and disease-free survival (1,2). Image guidance allows
55 for tumor dose escalation and normal tissue sparing, by enabling applicator and subsequent
56 source positioning to be tailored to individual tumor features and anatomy. High-quality
57 gynecologic (GYN) BT requires a skilled, coordinated multi-disciplinary team to carry out labor-
58 intensive workflows (3). Currently, clinicians rely on their BT experience, serial on-treatment
59 pelvic exams, and images from earlier time points to make decisions about applicator type prior
60 to the procedure. Quality assessment for BT treatment plans is challenging, as patient anatomy,
61 applicator choice, implant quality, and source loading pattern can all affect tumor coverage and
62 organ-at-risk (OAR) sparing. Currently there are no standardized tools to assist practitioners in
63 troubleshooting cases that do not achieve dosimetric goals. Furthermore, utilization of BT for
64 cervical cancer is declining, some of which could be due to the requirements of the sophisticated
65 workflow (4). This comes at a cost to patients, as a lack of BT is associated with reduced cause-
66 specific and overall survival (5). Additionally, BT remains the standard of care, as demonstrated
67 by a recent study that evaluated the use of stereotactic body radiation therapy (SBRT) in place of
68 BT for cervical cancer treatment and closed early due to concerns for toxicity (6).

69 Computational prediction of achievable dosimetric parameters could increase clinical
70 efficiency, improve treatment quality, and expand the accessibility and utilization of BT.
71 Population-based guidelines, and current protocols such as the ongoing clinical trial EMBRACE
72 II recommended dose constraints (7), provide clinicians with static plan quality metrics against
73 which to assess individual BT treatment plan quality. While useful for ensuring patients do not
74 exceed critical normal tissue limits, such guidelines are not patient-specific and only provide

75 limits. In analogous situations of external beam radiotherapy (EBRT) where only static
76 population-based limits are used as plan quality guidance, high degrees of plan quality variability
77 and excess dose to normal tissues have been observed (8,9).

78 Machine learning methods have been applied to EBRT to automate human-driven
79 processes through a technique known as knowledge-based planning (KBP) (10–14). Knowledge-
80 based dose estimation models are trained on large datasets of prior treatments and provide
81 patient-specific dosimetric predictions for new patients. Automated planning with KBP is
82 accomplished using patient-specific dose predictions to guide plan optimization. These
83 approaches have not been systematically translated to the unique challenges of intracavitary
84 GYN BT, where dosimetry is highly constrained by the implanted applicator and the degrees of
85 freedom for dose modulation are reduced. The purpose of this work was to explore the accuracy
86 of knowledge-based OAR dose estimation for high-dose rate (HDR) BT treatment of cervical
87 cancer. Using established external-beam knowledge-based DVH estimation methods (11), we
88 sought to accurately predict bladder, rectum, and sigmoid D_{2cc} for standard tandem-and-ovoid
89 (T&O) treatments. These dose estimations are an important precursor and step towards
90 knowledge-based planning in BT.

91 To our knowledge, this work is the first application of knowledge-based dose estimation
92 to GYN intracavitary BT where models are based only on contours of organs and target. This
93 approach could facilitate multi-institutional data-driven quality control, and increase BT
94 utilization by giving clinicians objective assurances that their dose distributions are of high
95 quality.

96

97 **Materials and Methods**

98 Model specification

99 The mathematical framework employed in this work for DVH estimation of OARs is
100 closely related to an approach developed for intensity-modulated radiation therapy (IMRT) (11).
101 The planning datasets consist of structure sets for the OARs, OAR_{ij} , for $i=1\dots N$ cases (where
102 “case” refers to a single fraction in a patient’s course of treatment) and $j=1\dots M$ OARs, and
103 corresponding structure-specific dose matrices $D[x, y, z; i, j]$, where (x, y, z) is the 3D-position
104 of a point that lies within the j^{th} structure. To facilitate equivalence we normalize dose in the i^{th}
105 case to its prescription dose, $\tilde{D}[x, y, z; i, j]=D[x, y, z; i, j]/D_{Rx_i}$.

106 Our model is built on the boundary distance feature that quantifies the minimum distance
107 r between any OAR volume element and the high-risk clinical target volume (HRCTV) target
108 (11). The primary assumption of this model is that the probability that a voxel in the j^{th} organ will

109 take a dose value between \tilde{D} and $\tilde{D}+\Delta\tilde{D}$ is given by $p_j(\tilde{D};r)\Delta\tilde{D}$, with $\int_0^{\infty} p_j(\tilde{D};r)d\tilde{D}=1$.

110 That this probability distribution is a function of r implies that any two points equidistant from
111 their respective HRCTV boundaries within the same organ will have the same normalized dose
112 distribution with respect to the prescription dose.

113 The practical consequences of these assumptions are that the dose-distance data of each
114 of the N cases can be pooled to generate an enlarged dataset used to estimate the ‘ensemble-
115 averaged’ dose-distance kernels $p_j(\tilde{D};r)$ for each of the $j=1-3$ OARs (bladder, rectum, and
116 sigmoid). Then, for a new case i_{N+1} , once we extract the differential volume of each OAR as a
117 function of r , $dV_{i_{N+1}j}/dr$, these kernels can be used to predict the differential DVH

118 $V'_{i_{N+1}}{}^{pred}(\tilde{D}_j) = \int dr \left(\frac{dV_{i_{N+1}j}}{dr} \right) p_j(\tilde{D}; r).$

119 In turn, this is transformed into the cumulative DVH,

120 $DVH_{i_{N+1}}{}^{pred}(\tilde{D}_j) = V_{i_{N+1}j}^{total} - \int_0^{\tilde{D}_j} dDV'_{i_{N+1}}{}^{pred}(\tilde{D}),$

121 where $V_{i_{N+1}j}^{total}$ is the total volume of the j^{th} OAR for the case. From this predicted cumulative DVH,
122 D_{2cc} metrics of the bladder, rectum, and sigmoid are extracted, since D_{2cc} is currently the only
123 standardized OAR DVH metric that is used to evaluate clinical plans.

124 Model training and validation

125 136 loco-regionally advanced cervical cancer patients, over a six-year period (2012-2018,
126 UCSD IRB Project #181609), treated with $N=456$ (356:100 training:validation ratio) T&O CT-
127 guided BT fractions were analyzed retrospectively in an integrated training-validation workflow
128 as illustrated in Figure 1. The 100 case validation set was composed of all 5 fractions of 10
129 patients completely independent of the training set, and 50 cases randomly sampled from the
130 remaining 126 patients (consisted of 2 treatment fractions from 9 patients, and single fractions
131 from 33 patients, for a total of 42 patients). The purpose of this was to evaluate model
132 performance on both totally independent patients, as well as independent treatment fractions
133 from patients used to train the model.

134 Single-fraction prescription doses were 4-8 Gy. Plans were created using institutional
135 dose criteria for external beam + BT equivalent dose in 2 Gy fractions (EQD2s), which were
136 originally based on the 2011 update to the ABS HDR BT guidelines for locally advanced
137 cervical cancer (15), and later updated to incorporate soft constraints from the ongoing
138 EMBRACE-II trial (7). Hard planning constraints include high-risk clinical target volume

139 (HRCTV) $D_{90}>85$ Gy, bladder $D_{2cc}<90$ Gy, rectum $D_{2cc}<75$ Gy, and sigmoid $D_{2cc}<75$ Gy. Soft
140 planning aims (recommended but not required) include bladder $D_{2cc}<80$ Gy, rectum $D_{2cc}<65$ Gy,
141 and sigmoid $D_{2cc}<70$ Gy. The HRCTV contour included residual disease at the time of BT and
142 the whole cervix. Our planning process consisted of the following steps. First, the T&O dwell
143 positions were set to a standard loading pattern, and then normalized to deliver prescription to
144 point A. Then radiation oncologists manually adjusted dwell positions or dragged isodose lines
145 to achieve target coverage while minimizing dose to OARs. During this tuning process, EQD2
146 values were evaluated on a spreadsheet to ensure planning objectives were met.

147 DVH estimation models were obtained by subdividing OARs into HRCTV boundary
148 distance sub-volumes (extending from overlapping with the HRCTV to 10.6 cm radially from the
149 HRCTV) and computing an ensemble-averaged differential DVH estimate from the training set
150 sub-volumes. Full DVH estimation was performed on all cases in the training and validation sets
151 by applying OAR sub-volume DVH models to each fraction's OARs. The proposed framework
152 was implemented in the form of in-house extensions to MIM (version 9.6.3, MIM Software Inc.,
153 Cleveland, Ohio, USA). The DVH predictions for any new case take less than 10 seconds.

154 Model performance was quantified by analyzing the residual $\Delta D_{2cc} = \text{Actual } D_{2cc} -$
155 Predicted D_{2cc} , where D_{2cc} is the absolute OAR dose for a single BT fraction. Standard deviation
156 over these residuals was taken as a measure of model error, as has been done for prior EBRT
157 KBP studies (10–13,16). Goodness-of-fit was measured by the Pearson correlation coefficient R
158 and the variance of the ΔD_{2cc} distribution. We chose to report most analysis and figures in
159 absolute dose, as absolute dose is more commonly used to evaluate OARs during treatment
160 planning, and thus is more clinically meaningful. To ensure this assumption was valid, metrics
161 were also computed for relative dose (i.e. dose normalized to prescription for that BT fraction).

162 Consistency between the distributions of ΔD_{2cc} for training and validation sets was checked with
163 an unpaired Student's t-test ($p < 0.01$ significance threshold).

164 Variance reduction via incorporation of continuous geometric features

165 In an attempt to uncover possible anatomic variability not captured by the boundary distance
166 approach, we identified a preliminary list of eleven geometric features suspected to have
167 additional predictive power, including:

- 168 1) HRCTV volume
- 169 2) An anterior-posterior asymmetry metric $AP_{\text{asymmetry}}$, defined as the furthest posterior
170 distance of the HRCTV boundary from the tandem minus the furthest anterior distance of
171 the HRCTV boundary from the tandem
- 172 3) Nine additional geometric features measuring OAR orientation relative to the base of the
173 HRCTV. The centroid of the inferior-most HRCTV slice was defined as the origin, and
174 the closest 2cc to the HRCTV was identified for each of the three OARs. The rationale
175 for this orientation feature is that the inferior-most slice of the HRCTV serves as a
176 surrogate for the top of the ovoids (the ovoids can contribute to dose deviations that
177 might not be captured by the HRCTV-driven model) and the closest 2cc of the OARs
178 likely correspond with the structure's highest dose values. The vector connecting
179 HRCTV base to the OAR's closest 2cc is then decomposed into the radial distance ρ ,
180 azimuth φ , and height (superior-inferior distance) z in the redefined coordinate system. A
181 negative z indicates the OAR's closest approach is inferior to the HRCTV and therefore
182 near the ovoids.

183 Some of these features are depicted in Figure 2. From this candidate feature set $F_{\text{candidate}}$, we
184 sought to identify the subset of predictor features $F_{\text{predictors}} \subseteq F_{\text{candidate}}$ that could explain error in

185 our initial model. We performed stepwise regression, iteratively adding and removing candidate
186 features to $F_{predictors}$, performing least squares multiple linear regression of ΔD_{2cc} on $F_{predictors}$,
187 and continuing until only the candidate features with statistically significant predictive power
188 remained in the predictor set ($p < 0.01$ threshold and Bonferroni corrections for multiple
189 hypothesis testing). This stepwise regression analysis was performed on all training cases, and
190 the end result was a linear model of ΔD_{2cc} as a function of a few significant variables. In order to
191 determine whether these variables could improve predictive accuracy, the linear model was
192 applied as a correction to predict D_{2cc} in the validation dataset.

193 Additional attempts at variance reduction via discrete categorical stratifications

194 In addition to the aforementioned set of candidate continuous features, we also considered
195 discrete categories $C_{candidate}$ that could potentially explain and reduce variance via stratification.
196 Our list of candidate categories fell into five classes, with the exact breakdown of our datasets by
197 categories listed in Table 1:

- 198 1) The chronological fraction number of a case within a patient's treatment, which defines
199 five distinct groups
- 200 2) The total number of prescribed fractions of the BT treatment
- 201 3) The tumor stage
- 202 4) The 'brachytype', a variable that attempts to capture case complexity. Although only T&O
203 fractions were included in the training and validation datasets, some patients were treated
204 with other applicators and/or needles for at least one other fraction. We suspect that the
205 use of needles or other applicators for some fractions might indicate more challenging
206 anatomy, and wanted to determine whether this affected model predictions. We defined
207 three distinct groups: group 1 corresponding to cases from patients who underwent

208 entirely T&O treatments, group 2 to patients who had either a tandem-and-ring (T&R) or
209 tandem-and-cylinder (T&C) implant at some point during treatment, and group 3 to
210 patients who received supplemental needles for at least one fraction.

211 5) The attending radiation oncologist, which resulted in five different groupings for this
212 dataset.

213 For each categorical variable considered, we tested for group-dependent differences in the
214 combined training and validation cohort in the distribution of ΔD_{2cc} via an ANOVA test with a
215 post-hoc Tukey's B analysis ($p < 0.01$ significance threshold for group-specific variation with
216 Bonferroni corrections for multiple hypothesis testing). All statistical data analysis was
217 performed using MATLAB (R2018a, MathWorks, Inc., Natick, Massachusetts, USA).

218

219 **Results**

220 Actual bladder D_{2cc} values for the combined training and validation cohort displayed a
221 [minimum:maximum] range of [1.65Gy:7.30Gy], with a mean \pm standard deviation of
222 4.64 ± 1.03 Gy. The corresponding statistics for rectum D_{2cc} were [1.12 Gy:6.50 Gy] and
223 3.58 ± 0.93 Gy, and for sigmoid D_{2cc} , they were [1.63Gy:6.58Gy] and 3.88 ± 0.86 Gy. Average
224 DVHs for each OAR, for both actual clinical plans and predictions, are shown in Figure 3.

225 The model predicted D_{2cc} to bladder, rectum and sigmoid to within 0.46-0.61 Gy, as
226 quantified by standard deviation (see Figure 4). Model accuracy did not statistically differ
227 between the validation and training datasets for bladder ($p=0.80$), rectum ($p=0.53$) or sigmoid
228 ($p=0.70$). When the validation dataset was separated into totally independent patients (group 1)
229 and independent treatment fractions from patients used to train the model (group 2), performance

230 metrics were similar (mean \pm standard deviation of $\Delta D_{2cc} = 0.06 \pm 0.45$ Gy, -0.02 ± 0.42 Gy
231 and -0.07 ± 0.47 Gy for bladder, rectum and sigmoid for group 1; and -0.08 ± 0.75 Gy, $-0.05 \pm$
232 0.43 Gy and -0.10 ± 0.50 Gy for group 2). Model accuracy did not significantly differ between
233 validation groups ($p > 0.25$). Mean and standard deviation over ΔD_{2cc} for dose normalized to
234 prescription for training (validation) were bladder = $-0.51 \pm 9.43\%$ ($0.13 \pm 9.38\%$), rectum =
235 $0.36 \pm 8.84\%$ ($-0.46 \pm 7.05\%$), and sigmoid = $-0.75 \pm 8.05\%$ ($-1.14 \pm 7.77\%$). Multiplying these
236 numbers by a 6-7 Gy prescription (the most common prescriptions of our dataset), these numbers
237 are similar to those obtained for absolute dose.

238 The results of the categorical stratification analyses on the combined training and
239 validation cohorts for various group variables are reported in Table 2. The ANOVA and post-hoc
240 analyses revealed that ΔD_{2cc} values significantly varied between radiation oncologists for
241 bladder ($p < 0.001$) and rectum ($p < 0.001$) (see Figure 5). No significant differences were found
242 between any other stratifications. To test whether inter-practitioner differences in OAR dose
243 might be related to differences in target coverage, we ran an ANOVA and post-hoc analysis for
244 D90, dose to 90% of the HRCTV, normalized to prescription. As indicated in Figure 4, while
245 there are physician-dependent differences in coverage, these differences are not clearly related to
246 the corresponding differences seen for ΔD_{2cc} metrics.

247 The stepwise linear regression highlighted up to one significant variable correcting each
248 organ model. Bladder ΔD_{2cc} was correlated with $AP_{\text{asymmetry}}$, rectum ΔD_{2cc} was correlated with
249 z_{rectum} , and sigmoid ΔD_{2cc} was correlated with none of the analyzed features (regression equations
250 and adjusted R-squared shown in Supplementary Material, Table S1). The results of the stepwise
251 multiple linear regression suggest that certain geometric features have nonzero predictive

252 correlation with ΔD_{2cc} , but ultimately these corrections made on average very modest ~ 0.02 Gy
253 improvements in ΔD_{2cc} prediction accuracy as quantified by the standard deviation (σ) and
254 correlation coefficient R (Table 3).

255

256 **Discussion**

257 Machine learning is thus far relatively unexplored in the BT realm. One study applied
258 machine learning to automate planning for prostate low dose rate BT (17). For HDR BT, several
259 recent papers have investigated the use of advanced computational methods in multi-objective
260 optimization criteria (18–20), and multiple pilot studies (21–23) have successfully automated
261 various aspects of treatment planning. Damato *et al* (24) developed simple mathematical models
262 to predict bladder and rectum D_{2cc} for interstitial GYN BT, using a dataset of 20 patients.
263 However, to our knowledge this is the first study that applies machine learning to patient-specific
264 dosimetric prediction in intracavitary GYN BT. In contrast to the interstitial GYN work (24), we
265 had a much larger patient group and thus were able to validate our model on an independent
266 dataset, and our models include only geometric inputs.

267 As shown in Figure 4, our knowledge-based DVH estimation system predicts D_{2cc} to
268 OARs to within 0.46-0.61 Gy standard deviation. This amounts to a ± 0.9 -1.2 Gy 95% confidence
269 interval for each BT fraction. Model performance did not significantly differ between the training
270 and two validation sets, indicating that the model is not skewed towards patients included in the
271 training set, and does not suffer from overfitting. Although the entire OAR DVH is not
272 considered in current cervical brachytherapy practice and thus was not a focus of this work, the
273 model did predict reasonable DVHs on average, as shown in Figure 3. In its current form, the

274 model uses only contour information from post-implant CT imaging and does not require
275 applicator geometry, effectively providing an external reference for expected T&O dosimetry.
276 The value of this is that any institution could input their HRCTV and OAR contours and receive
277 a prediction for the dose they could expect for a given T&O implant. In addition, because of the
278 non-reliance on applicator geometry, this approach could be extended to create decision support
279 tools that could identify cases where T&O applicators alone could/could not meet dosimetric
280 constraints. Since interstitial needle implantation is challenging, increases treatment time and can
281 reduce patient comfort, it would be valuable to identify cases that do not need needles up front.

282 The analysis of relative dose resulted in model performance metrics that were similar to
283 those in absolute dose, using an average per fraction prescription of ~6-7 Gy to convert between
284 the two. For example, the standard deviations of ΔD_{2cc} ranged from 7.1 to 9.4% (0.46 to 0.61 Gy
285 in absolute dose), and mean ΔD_{2cc} ranged from -1.14 to 0.36% (-0.07 to 0.02 Gy). In addition,
286 model accuracy did not significantly differ between patients treated with different total numbers
287 of fractions (and by extension, cases with different prescriptions). Based on these results, we feel
288 it is valid to train and apply these models on cases with different prescriptions.

289 Notably, the predictive accuracy of ΔD_{2cc} to within 0.46-0.61 Gy standard deviation is
290 comparable to the range of inter-practitioner differences in ΔD_{2cc} means, e.g. [-0.69 Gy, 0.1 Gy]
291 for rectum. There are numerous unaccounted for inter-practitioner variations that could influence
292 dose, including differences in applicator loading, updates in target and OAR constraints over
293 time, variability in contouring and vaginal packing, differences in patient groups, and variations
294 in internal optimization stopping criteria, which is further complicated by the disconnect between
295 isodose tuning and DVH dose evaluation. The fact that our model already predicts estimation
296 error to within inter-practitioner variability in spite of these complexities is promising, and

297 suggests that the model can be used for plan quality control. In fact, the model was able to
298 identify a case (see * in Figure 6A) that featured a non-ideal implant due to difficulties with
299 tandem insertion through a stenotic os into an anteverted uterus. In later fractions, where
300 implants were improved (e.g. Figure 6B), the actual doses were in better agreement with the
301 model-predicted doses (ΔD_{2cc} for bladder ranged from 1.07-2.05 Gy for fractions 2-4, while
302 ΔD_{2cc} for fraction 1 was 3.52 Gy). This suggests that the model could help physicians decide
303 whether a re-implant is warranted for challenging cases. It should be noted that although
304 variability was observed between practitioners, nearly all clinical plans met our institutional dose
305 constraints.

306 The HRCTV and OAR contours used in this study were primarily CT-based. It stands to
307 question whether the current models would be directly applicable for MR-based contouring and
308 planning. MR-based tumor volumes for cervical cancer have been shown to be smaller than
309 those drawn on CT (25). Since the model relies only on the extracted contours, it should still
310 provide accurate predictions for any given HRCTV.

311 There are limitations to our presented approach. The study was restricted to a single
312 institution and, presently, only considers standard T&O cases. Like similar EBRT KBP methods
313 (11,14), the target coverage is taken as a set variable, and therefore the model cannot be used to
314 predict target coverage, or predict optimal target and OAR dose tradeoffs. The identification of
315 any significant geometric predictors of ΔD_{2cc} hints that more sophisticated accounting of
316 HRCTV and applicator geometry could yield more accurate predictions. Figure 6 shows
317 examples of a few geometric features that are not well captured by the simple HRCTV
318 boundary-distance model, such as asymmetry of the HRCTV with respect to the tandem and
319 dose from the ovoids. However, it is evident that a linear correction for these features is

320 insufficient; although model error was reduced in the training dataset by 0-4 cGy after the
321 correction, there was no improvement in predictive accuracy in the validation set, leading to
322 concerns of over-fitting. Regardless, despite the model's reliance on a simplistic assumption of
323 equivalent dose fall-off for points within an organ that are equidistant from the target (which is
324 arguably more applicable to EBRT treatment plans), it seems to perform quite well. Future work
325 will explore voxel-based dose prediction that accounts for relative positioning of targets, OARs
326 and all applicator components.

327 Despite the current model's limitations, the ~0.5 Gy prediction accuracy demonstrates
328 that the model could function as a multi-institutional quality control tool for T&O BT planning,
329 since it can compute BT predictions from contours alone. Predictions are produced fully within
330 the MIM environment and require only the structure set of an RT DICOM, so any institution
331 with MIM could upload a structure set for a patient and receive dose predictions with the click of
332 a button. As seen in the context of multi-institutional clinical trials of EBRT (9,26), objective
333 measures of plan quality can highlight previously uncontrolled quality variability across multiple
334 institutions. Patient-specific dose predictions can not only quantify unknown quality variations in
335 BT practice, but also provide a means to reduce inter-practitioner variability. Future work will
336 extend these models to other applicators and intracavitary/interstitial hybrid cases and examine
337 whether predictions could guide further plan optimization and improve plan quality by re-
338 planning cases with large discrepancies between predicted and actual dose. Finally, we will
339 deploy this tool in the multi-institutional context and utilize dose predictions for fully-automated
340 BT planning.

341 In summary, we have adapted knowledge-based dose prediction methods to predict OAR
342 DVHs and, in particular, the critical OAR D_{2cc} quality metric for GYN brachytherapy. To our

343 knowledge, this is the first such application of knowledge-based methods to GYN brachytherapy
344 and could form the basis for treatment plan quality control and automated brachytherapy
345 planning.

346

347 **Disclosure**

Dr. Meyers, Moore and Mayadev report grants from Padres Pedal the Cause, during the conduct of the study. Dr. Moore acknowledges funding support from AHRQ (R01 HS025440-01), has a patent Developing Predictive Dose-Volume Relationships for a Radiotherapy Treatment licensed to Varian Medical Systems, and a patent Knowledge-based prediction of three-dimensional dose distributions pending. In addition, Drs. Moore, Brown and Scanderbeg acknowledge research funding, travel support, and honoraria from Varian Medical Systems, outside the submitted work. Dr. Mayadev reports personal fees from AstraZeneca, grants from NRG Oncology, grants from GOG Foundation, personal fees from Varian Medical Systems, outside the submitted work. Dr. Simon reports personal fees from Courage Health, Inc., outside the submitted work.

Acknowledgments:

We thank James Murphy for helpful discussions.

348

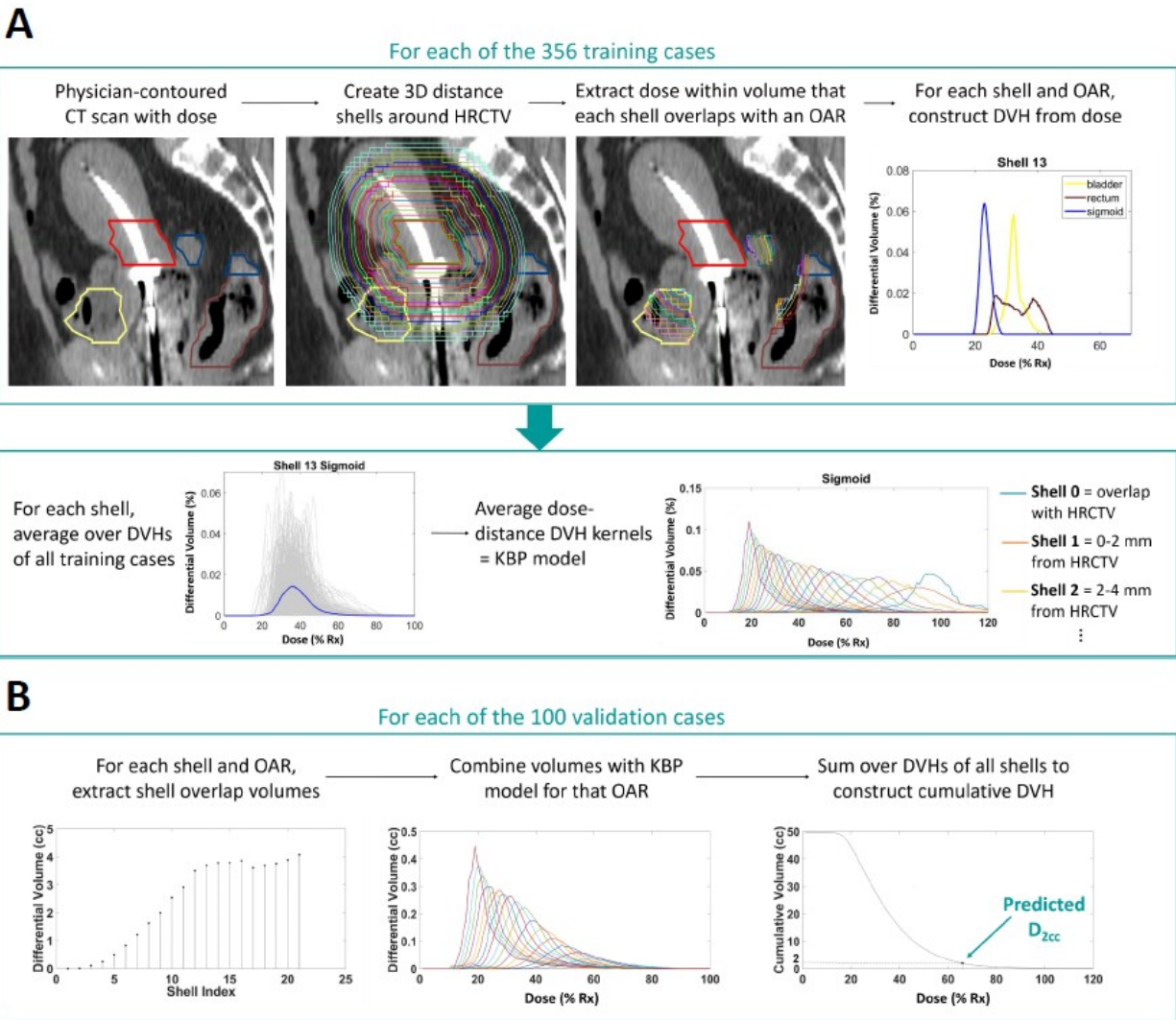
Funding: This work was supported by a Translational Cancer Research Award from Padres Pedal the Cause.

349 References

- 350 1. Hanks GE, Herring DF, Kramer S. Patterns of care outcome studies. Results of the national practice
351 in cancer of the cervix. *Cancer*. 1983 Mar 1;51(5):959–67.
- 352 2. Eifel PJ, Moughan J, Erickson B, Iarocci T, Grant D, Owen J. Patterns of radiotherapy practice for
353 patients with carcinoma of the uterine cervix: a patterns of care study. *Int J Radiat Oncol Biol Phys*.
354 2004 Nov 15;60(4):1144–53.
- 355 3. Mayadev J, Qi L, Lentz S, Benedict S, Courquin J, Dieterich S, et al. Implant time and process
356 efficiency for CT-guided high-dose-rate brachytherapy for cervical cancer. *Brachytherapy*. 2014
357 Jun;13(3):233–9.
- 358 4. Ma TM, Harkenrider MM, Yashar CM, Viswanathan AN, Mayadev JS. Understanding the
359 underutilization of cervical brachytherapy for locally advanced cervical cancer. *Brachytherapy*.
360 2019 Jun;18(3):361–9.
- 361 5. Mayadev J, Klapheke A, Yashar C, Hsu I-C, Kamrava M, Mundt AJ, et al. Underutilization of
362 brachytherapy and disparities in survival for patients with cervical cancer in California. *Gynecol*
363 *Oncol*. 2018;150(1):73–8.
- 364 6. Albuquerque K, Tumati V, Lea J, Ahn C, Richardson D, Miller D, et al. A Phase II Trial of
365 Stereotactic Ablative Radiation Therapy as a Boost for Locally Advanced Cervical Cancer. *Int J*
366 *Radiat Oncol Biol Phys*. 2020 01;106(3):464–71.
- 367 7. Pötter R, Tanderup K, Kirisits C, de Leeuw A, Kirchheiner K, Nout R, et al. The EMBRACE II
368 study: The outcome and prospect of two decades of evolution within the GEC-ESTRO GYN
369 working group and the EMBRACE studies. *Clin Transl Radiat Oncol*. 2018 Feb;9:48–60.
- 370 8. Nelms BE, Chan MF, Jarry G, Lemire M, Lowden J, Hampton C, et al. Evaluating IMRT and
371 VMAT dose accuracy: practical examples of failure to detect systematic errors when applying a
372 commonly used metric and action levels. *Med Phys*. 2013 Nov;40(11):111722.
- 373 9. Moore KL, Schmidt R, Moiseenko V, Olsen LA, Tan J, Xiao Y, et al. Quantifying Unnecessary
374 Normal Tissue Complication Risks due to Suboptimal Planning: A Secondary Study of RTOG
375 0126. *Int J Radiat Oncol Biol Phys*. 2015 Jun 1;92(2):228–35.
- 376 10. Moore KL, Brame RS, Low DA, Mutic S. Experience-based quality control of clinical intensity-
377 modulated radiotherapy planning. *Int J Radiat Oncol Biol Phys*. 2011 Oct 1;81(2):545–51.
- 378 11. Appenzoller LM, Michalski JM, Thorstad WL, Mutic S, Moore KL. Predicting dose-volume
379 histograms for organs-at-risk in IMRT planning. *Med Phys*. 2012 Dec;39(12):7446–61.
- 380 12. Shiraishi S, Tan J, Olsen LA, Moore KL. Knowledge-based prediction of plan quality metrics in
381 intracranial stereotactic radiosurgery. *Med Phys*. 2015 Feb;42(2):908.
- 382 13. Shiraishi S, Moore KL. Knowledge-based prediction of three-dimensional dose distributions for
383 external beam radiotherapy. *Med Phys*. 2016 Jan;43(1):378.

- 384 14. Ge Y, Wu QJ. Knowledge-based planning for intensity-modulated radiation therapy: A review of
385 data-driven approaches. *Med Phys*. 2019 Jun;46(6):2760–75.
- 386 15. Viswanathan AN, Beriwal S, De Los Santos J, Demanes DJ, Gaffney D, Hansen J, et al. The
387 American Brachytherapy Society Treatment Recommendations for Locally Advanced Carcinoma of
388 the Cervix Part II: High Dose-Rate Brachytherapy. *Brachytherapy*. 2012;11(1):47–52.
- 389 16. Cornell M, Kaderka R, Hild SJ, Ray XJ, Murphy JD, Atwood TF, et al. Noninferiority Study of
390 Automated Knowledge-Based Planning Versus Human-Driven Optimization Across Multiple
391 Disease Sites. *International Journal of Radiation Oncology*Biophysics*Physics [Internet]*. 2019 Oct
392 31 [cited 2020 Jan 6]; Available from:
393 <http://www.sciencedirect.com/science/article/pii/S0360301619339586>
- 394 17. Nicolae A, Morton G, Chung H, Loblaw A, Jain S, Mitchell D, et al. Evaluation of a Machine-
395 Learning Algorithm for Treatment Planning in Prostate Low-Dose-Rate Brachytherapy. *Int J Radiat
396 Oncol Biol Phys*. 2017 15;97(4):822–9.
- 397 18. Bélanger C, Cui S, Ma Y, Després P, Adam M Cunha J, Beaulieu L. A GPU-based multi-criteria
398 optimization algorithm for HDR brachytherapy. *Phys Med Biol*. 2019 May 8;64(10):105005.
- 399 19. Guthier CV, Aschenbrenner KP, Müller R, Polster L, Cormack RA, Hesser JW. Real-time inverse
400 high-dose-rate brachytherapy planning with catheter optimization by compressed sensing-inspired
401 optimization strategies. *Phys Med Biol*. 2016 21;61(16):5956–72.
- 402 20. Luong NH, Alderliesten T, Pieters BR, Bel A, Niatsetski Y, Bosman PAN. Fast and insightful bi-
403 objective optimization for prostate cancer treatment planning with high-dose-rate brachytherapy.
404 *Applied Soft Computing*. 2019 Nov 1;84:105681.
- 405 21. Zhou Y, Klages P, Tan J, Chi Y, Stojadinovic S, Yang M, et al. Automated high-dose rate
406 brachytherapy treatment planning for a single-channel vaginal cylinder applicator. *Phys Med Biol*.
407 2017 07;62(11):4361–74.
- 408 22. Deist TM, Gorissen BL. High-dose-rate prostate brachytherapy inverse planning on dose-volume
409 criteria by simulated annealing. *Phys Med Biol*. 2016 Feb 7;61(3):1155–70.
- 410 23. Shen C, Gonzalez Y, Klages P, Qin N, Jung H, Chen L, et al. Intelligent inverse treatment planning
411 via deep reinforcement learning, a proof-of-principle study in high dose-rate brachytherapy for
412 cervical cancer. *Phys Med Biol*. 2019 May 29;64(11):115013.
- 413 24. Damato AL, Viswanathan AN, Cormack RA. Validation of mathematical models for the prediction
414 of organs-at-risk dosimetric metrics in high-dose-rate gynecologic interstitial brachytherapy. *Med
415 Phys*. 2013 Oct;40(10):101711.
- 416 25. Viswanathan AN, Erickson B, Gaffney DK, Beriwal S, Bhatia SK, Lee Burnett O, et al. Comparison
417 and consensus guidelines for delineation of clinical target volume for CT- and MR-based
418 brachytherapy in locally advanced cervical cancer. *Int J Radiat Oncol Biol Phys*. 2014 Oct
419 1;90(2):320–8.

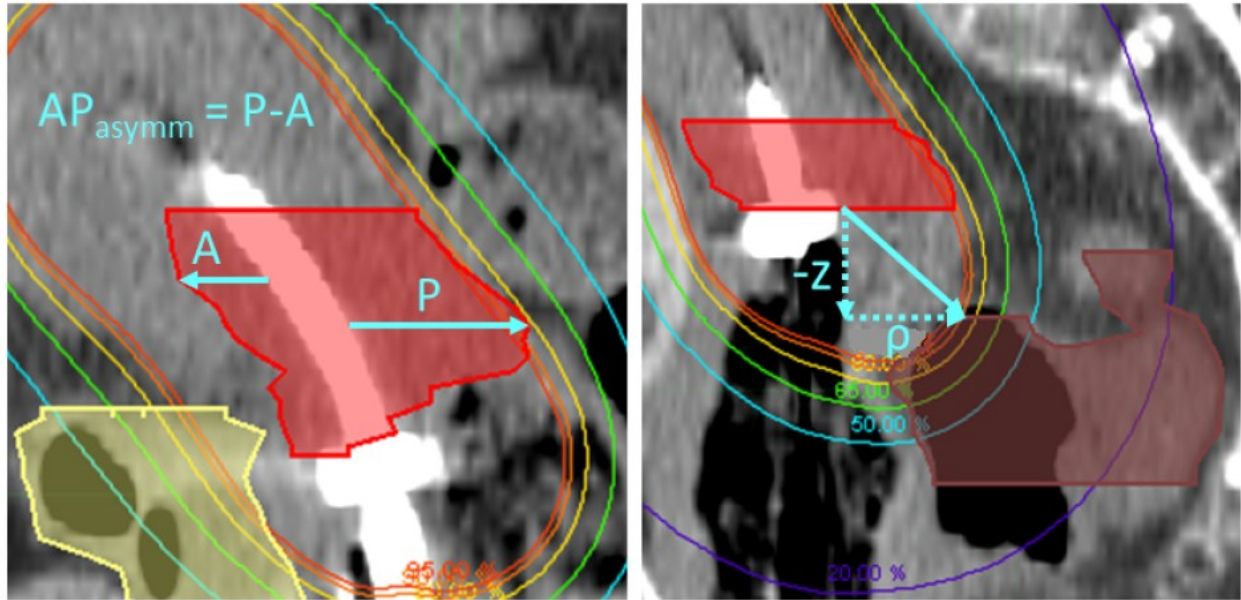
420 26. Li N, Carmona R, Sirak I, Kasaova L, Followill D, Michalski J, et al. Highly Efficient Training,
 421 Refinement, and Validation of a Knowledge-based Planning Quality-Control System for Radiation
 422 Therapy Clinical Trials. *Int J Radiat Oncol Biol Phys.* 2017 01;97(1):164–72.



423
 424 **Figure 1.** Methodology and workflow applied to A) train the model, and B) validate on a
 425 separate dataset.

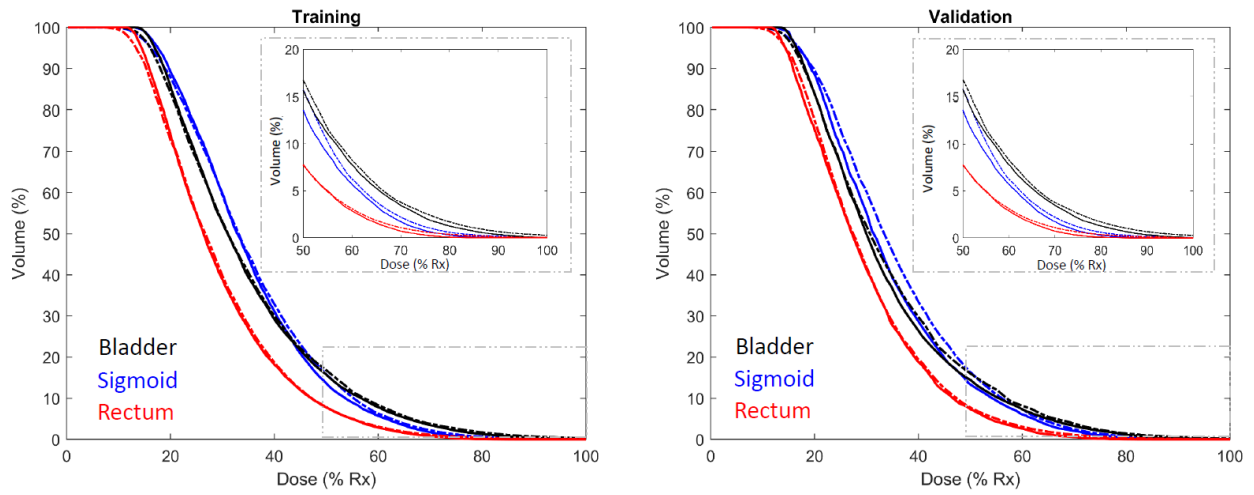
426

427



428 | **Figure 2.** Illustration of some of the geometric features and how they were defined, including the
429 anterior-posterior asymmetry metric, $AP_{\text{asymmetry}}$ (left), which quantifies how well the tandem was
430 centered in the HRCTV, superior-inferior distance, z , and radial distance ρ (right), which
431 identify the relative positioning of the closest 2cc of an OAR to the base of the HRCTV.

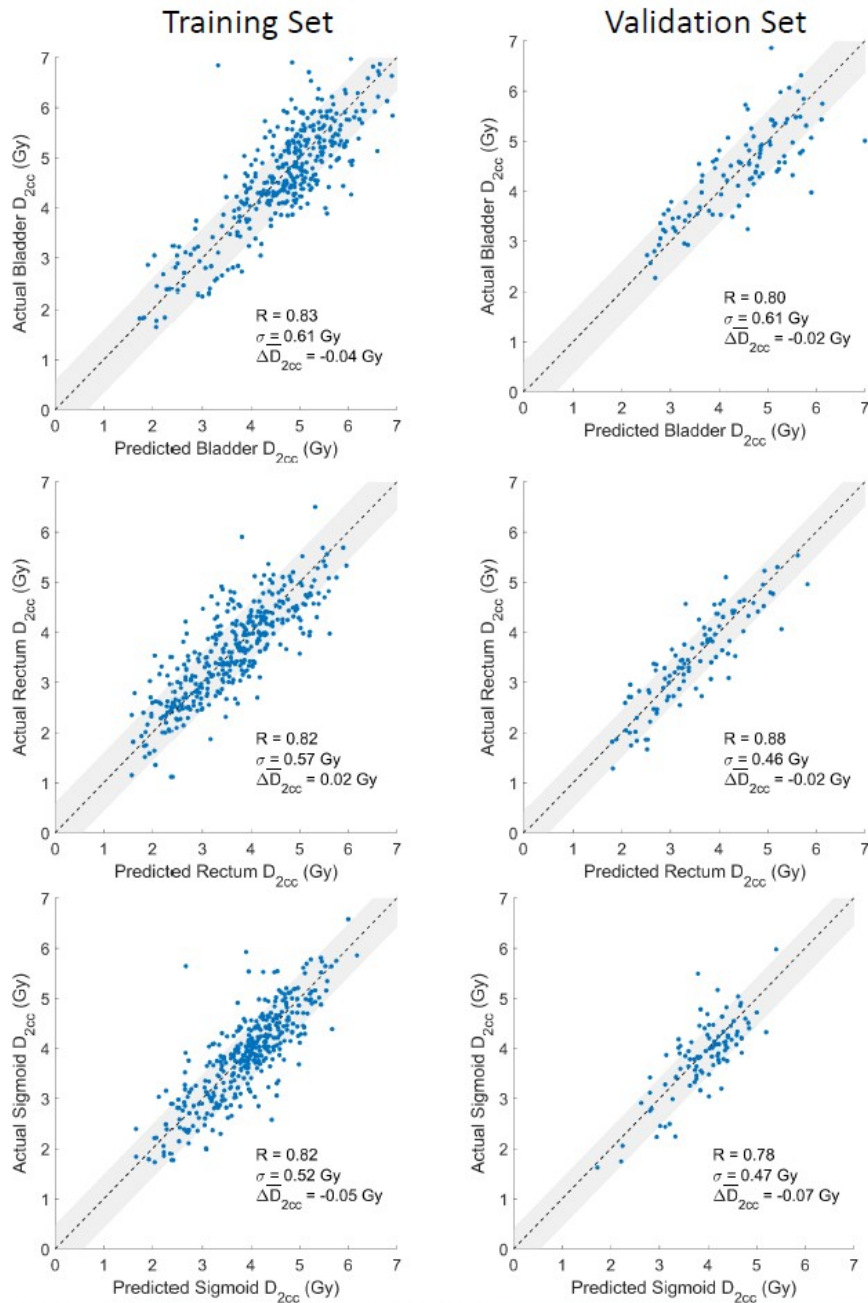
432



433

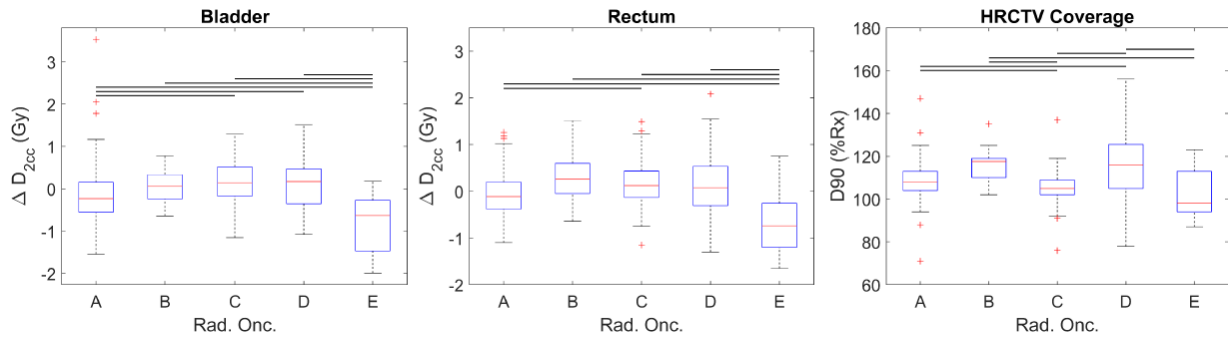
434 **Figure 3.** Actual (solid line) and predicted (dotted line) OAR DVHs, averaged over all cases in
 435 training (A) and validation (B) datasets.

436



437

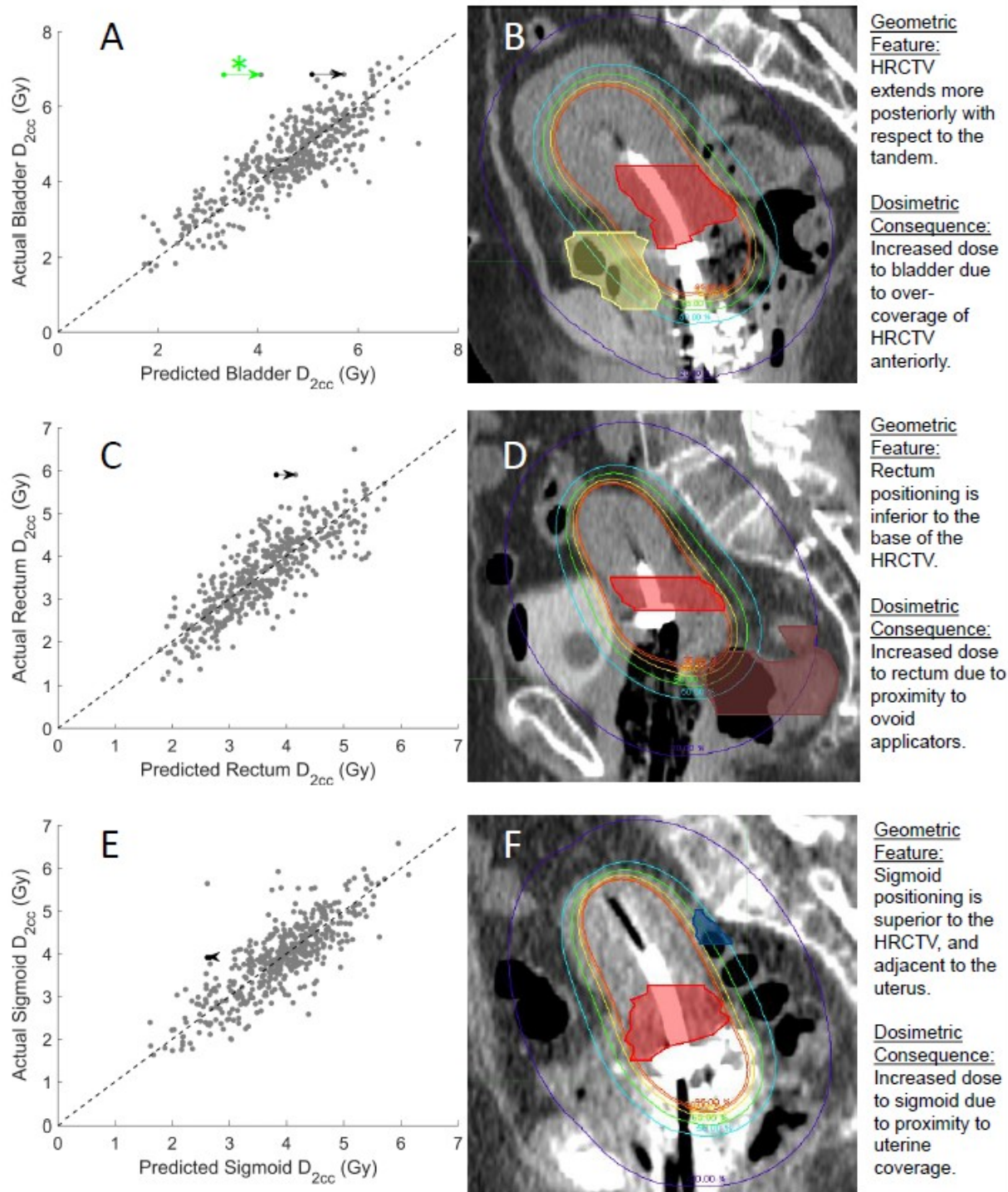
438 | **Figure 4.** Actual vs. predicted D_{2cc} for each organ for training and validation datasets, along
 439 | with Pearson correlation coefficients (R), standard deviation (indicated by σ as well as grey
 440 | colorwash) and mean of ΔD_{2cc} 's (equal to zero for the training set due to bias subtraction). Black
 441 | lines indicate hypothetical perfect model predictions.



443

444 **Figure 5.** Box-and-whisker plots showing physician-dependent variation in ΔD_{2cc} for bladder and
 445 rectum, along with corresponding variation in the HRCTV coverage metric D90. Black line
 446 segments connect pairs of physicians whose average ΔD_{2cc} or D90 values significantly differed at
 447 the confidence level $p < 0.01$, after accounting for multiple-comparison corrections.

448



449

F

450 **figure 6.** (A, C, E) show pooled plots of both the training and validation dataset predictions after
 451 geometric correction, compared to the actual values. (B, D, E) display example cases that

452 featured a large deviation between actual and predicted D_{2cc} , along with explanations of the
453 underlying geometric features that likely led to these discrepancies. The black arrow in each plot
454 shows how each of these cases changed with the geometric correction. The most extreme outlier
455 in (A) (indicated by the green arrow and *) corresponded to a first-fraction case that featured a
456 non-ideal implant due to difficulties with tandem insertion through challenging anatomy. The
457 implants improved for later fractions (e.g. (B), which was the second fraction of the same
458 patient), and as a result the difference between actual and predicted dose was much smaller.

459

460 **Table 1.** Breakdown of training and validation data by various categorical features, including the
 461 stage, attending radiation oncologist, total number of fractions and fraction number of the case.
 462 Some patients received T&O for all fractions of their treatment (“All T&O”), while other
 463 patients (“Component T&O”) had at least one fraction that was treated with a different applicator
 464 (tandem and cylinder (T&C) or tandem and ring (T&R)), or needles. Although only T&O
 465 fractions were included in training and validation datasets, the “Brachytype” provides a
 466 breakdown of the number of cases that corresponded to patients that fell into each of these
 467 categories.

468

Number of patients	Training (P = 114)	Validation (P= 52)	Total (P = 126)
Stage			
T1	35	11	40
T2	51	26	57
T3	25	15	26
T4	3	0	3
Prescribed total number of fractions			
2	1	0	1
3	5	4	6
4	54	14	54
5	54	34	64
Number of cases	Training (N = 356)	Validation (N = 100)	Total (N = 456)
Physician			
A	154 (43 %)	44 (44 %)	198 (44 %)
B	16 (5 %)	8 (8 %)	24 (5 %)
C	101 (28 %)	18 (18 %)	119 (26 %)
D	69 (19 %)	27 (27 %)	96 (21 %)
E	16 (5 %)	3 (3 %)	19 (4 %)
Brachytype			
All T&O	304 (85 %)	96 (96 %)	400 (88 %)
Component T&O	52 (15 %)	4 (4%)	56 (12 %)
- T&C	- 13 (4 %)	- 2 (2%)	- 15 (3 %)
- T&R	- 16 (6 %)	- 1 (1%)	- 17 (5 %)
- Needles	- 23 (5 %)	- 1 (1%)	- 24 (4 %)

Fraction Number

1	87 (24 %)	18 (18%)	105 (23 %)
2	84 (24 %)	19 (19%)	103 (23 %)
3	73 (21 %)	28 (28%)	101 (22 %)
4	72 (20 %)	19 (19%)	91 (20 %)
5	40 (11 %)	16 (16%)	56 (12 %)

469

470

471

472 **Table 2.** The results of categorical stratification analysis indicate that, after
 473 Bonferroni corrections, only stratification by radiation oncologist for bladder and
 474 rectum yields significant differences in ΔD_{2cc} (as indicated by bold text).

	ΔD_{2cc} p-Value		
	Bladder	Rectum	Sigmoid
Physician	1.6×10^{-12}	6.6×10^{-11}	1.9×10^{-3}
Brachytype	0.30	0.08	0.05
Tumor Stage	0.98	0.46	0.34
Fraction Number	0.60	0.50	0.33
Total Number of Fractions	0.77	0.80	0.71

475

476

477

478

479

480 **Table 3.** A comparison of model performance metrics on both the training and validation sets,
 481 both before and after including geometric corrections.

482

OAR	Model Performance	Training Set (N=356)		Validation Set (N=100)	
		Pre-correction	Post-correction	Pre-correction	Post-correction
Bladder	<D _{2cc} >	-0.04 Gy	0.00 Gy	-0.02 Gy	0.02 Gy
	R	0.83	0.85	0.80	0.80
	σ	0.61 Gy	0.57 Gy	0.61 Gy	0.61 Gy
Rectum	<D _{2cc} >	0.02 Gy	0.00 Gy	-0.01 Gy	-0.02 Gy
	R	0.82	0.83	0.89	0.86
	σ	0.57 Gy	0.53 Gy	0.43 Gy	0.49 Gy
Sigmoid	<D _{2cc} >	-0.05 Gy	0.00 Gy	-0.07 Gy	-0.02 Gy
	R	0.82	0.82	0.79	0.78
	σ	0.52 Gy	0.52 Gy	0.47 Gy	0.47 Gy

483

484

485

486

487

488 **Table S1.** Displayed are the best-fit linear regression models of ΔD_{2cc} to selected
 489 geometric features for each of the three OARs. Mean estimates of the dominant
 490 coefficients are listed, along with the corresponding standard errors (S.E.). The
 491 adjusted R-squared, which measures the goodness-of-fit adjusted for the number of
 492 fitting parameters, is also listed.
 493

494

OAR	Regression Equation (Coefficients listed as Mean \pm S.E.)	Adj. R-Squared
Bladder	$\Delta D_{2cc} = (-0.11 \pm 0.03) + (0.05 \pm 0.01) AP_{\text{asymmetry}}$	0.13
Rectum	$\Delta D_{2cc} = (-0.00 \pm 0.03) - (-0.19 \pm 0.02) Z_{\text{rectum}}$	0.14
Sigmoid	$\Delta D_{2cc} = (-0.05 \pm 0.03)$	0.00

495

496

497

498

499

500

501

502

503

504

505

506

507